A HYPERSPECTRAL PHOTON TRANSPORT SYSTEM TO SIMULATE IMAGING SPECTROMETER OBSERVATIONS OF TERRESTRIAL ECOSYSTEMS

Gregory P. Asner

1. Introduction

Physical models of radiation reflected by an object or objects can aid in the analysis and interpretation of radiative measurements collected by field, airborne and spaceborne optical sensors. In the case of vegetation and soils, many photon transport models have been developed that range from analytical-empirical algorithms to highly mechanistic radiative transfer and ray tracing models (e.g., Goel 1988, Myneni and Asrar 1993). Some of these models have been numerically inverted to estimate vegetation and soil properties from optical remote sensing observations (e.g., Privette et al. 1996, Asner et al. 1998, 1999, and others). To date, only a few models have been specifically developed to simulate high spectral resolution sensors (Jacquemoud et al. 1993, Asner et al. 1999). A major difficulty in designing a physical model for high spectral resolution applications lies in the practical trade-off between model speed and realism. The most "realistic" 3-dimensional ray tracing and radiative transfer codes are often prohibitively slow and are thus difficult to apply when simulating many spectral bands or many pixels. Instruments such as the Airborne Visible and Infrared Imaging Spectrometer (AVIRIS) and the forthcoming EO-1 Hyperion spectrometer create images of ~ 220 spectral channels and many thousands of pixels. Simulation of AVIRIS and Hyperion scenes is a major computational challenge. Inversion of a physical model to estimate surface properties from spectrometer data is even more challenging. Thus, an ideal photon transport model of hyperspectral observations is one that is computationally efficient yet which physically embodies the major sources of variation in land-surface reflectance.

No integrated "systems" have been designed to accurately represent both the physical *and* ecological controls governing the dominant sources of variation in land-surface (or ecosystem) reflectance. Many models can do a reasonable job of simulating photon transport in simple, theoretical canopies, but the leap from these models to real world applications requires significant input from the ecological and biogeochemical points of view (Asner 1998). In particular, temporal and spatial variation in biochemical and biophysical properties of vegetation can render physical models useless if the ecological and biogeochemical range of variability is not well represented in an analysis.

As a step toward addressing these issues, a photon transport system was developed to simulate pixel- and regional-scale variability in hyperspectral reflectance/radiance signatures as observed by AVIRIS and EO-1 Hyperion sensors. The model incorporates six major components needed to realistically simulate these signatures: (1) a multi-biome database of the hyperspectral scattering properties of plant tissues including foliage, woody material, and litter; (2) a database of soil surface hyperspectral reflectance variability by soil taxonomic sub-order; (3) a database of plant structural and architectural properties at the canopy and landscape scales; (4) a physically-based, multi-stream canopy radiative transfer model; (5) a landscape inter-canopy shadowing model; and (6) an atmospheric radiative transfer code. This system of models and databases was then used to simulate variation in pixel-level reflectance and top-of-atmosphere radiance for a variety of environments ranging from arid shrubland to grassland to tropical forest (Figure 1). The model provides a means to estimate sources of variability in hyperspectral signatures under changing biological, geophysical, and atmospheric conditions. It also allows for the estimation of surface parameters from AVIRIS data using an inverse modeling approach. Examples of these applications are presented, and planned steps to improve the model are highlighted.

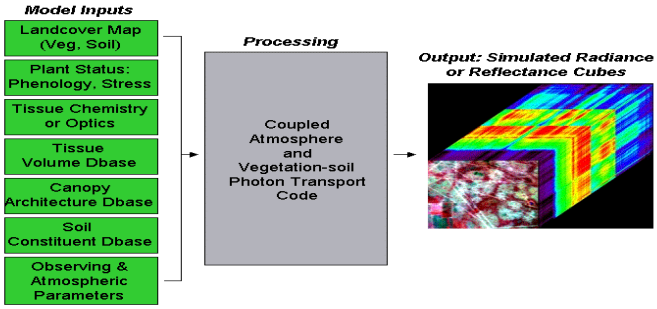

Figure 1. Schematic of hyperspectral photon transport system, including input parameters and databases.

Department of Geological Sciences and Environmental Studies Program, University of Colorado, Boulder, CO

2. Model Description

2.1 Radiative Transfer at the Canopy Scale

As with many canopy radiative transfer models, the reflectance is divided into three major parts: (1) radiation that is not scattered by vegetative tissues, (2) singly scattered radiation, and (3) radiation that undergoes multiple scattering:

$$\rho_{canopy}(\Omega'\Omega) = \rho_{unscat}(\Omega'\Omega)) + \rho_{\sin gsc}(\Omega'\Omega)) + \rho_{multsc}(\Omega'\Omega) \quad (1)$$

where Ω' represents the geometry of illumination in both zenith ($\mu'=\cos(\theta')$) and azimuth (ϕ') directions, and Ω represents the observer's geometric position in zenith ($\mu=\cos(\theta)$) and azimuth (ϕ) directions. In the following sections, equation (1) is broken down into components describing the transfer of incoming radiation between plant parts (e.g., foliage, wood, litter), the soil/litter surface, and the atmosphere. The primary components of the canopy-level radiative transfer model were provided by Verstraete et al. (1990) and Iaquinta and Pinty (1994), but were reformulated to allow for any number of tissue types (e.g., green leaves, wood, litter). Further modifications were made to enhance the speed of the algorithm. Here, I present the main components of the model to show where multiple vegetation tissues are incorporated for hyperspectral applications.

2.2 Photon Scattering by Plant Tissues

The spectral and angular distribution of scattered flux at the tissue level plays an important role in canopy-level scattering processes. This distribution can be described by the scattering phase function for a hypothetical single-sided tissue element of foliage, wood, litter, etc. If incident radiation from a direction Ω' strikes an infinitesimally small tissue area $d\sigma_T$ whose orientation is Ω_T, and if the intensity of that radiation is $I(\Omega')$, then the amount of radiant energy contained in the solid angle about Ω' that interacts with the tissue element within an interval of time (dt) is:

$$dE'_T = I(\Omega')\,|\cos\Omega_T\Omega'|\,d\sigma_T d\Omega' dt \quad (2)$$

where $\cos\Omega_T\Omega' = \cos\theta'\cos\theta_T + \sin\theta'\sin\theta_T\cos(\phi'-\phi_T)$. A fraction of this incident energy is scattered, and the remainder is absorbed. We can then denote the scattering phase function of tissue types:

$$f(\Omega,\Omega';\Omega_T)d\Omega = \frac{dE_{T\omega}}{dE'_T} \quad (3)$$

where the numerator represents the amount of energy scattered into a solid angle about the direction Ω. Tissue scattering phase functions are modeled as a Lambertian distribution for each side of the leaf, wood or litter tissue element. The equation for bi-Lambertian scattering by each element is:

$$f(\Omega',\Omega;\Omega_T) = \begin{cases} (r_T\,|\cos\Omega_T\Omega|)/\pi; & (\cos\Omega_T\Omega)(\cos\Omega_T\Omega') < 0 \\ (t_T\,|\cos\Omega_T\Omega|)/\pi; & (\cos\Omega_T\Omega)(\cos\Omega_T\Omega') > 0 \end{cases} \quad (4)$$

Here, r_T is the scattered energy due to reflection, and t_T is the scattered energy that is transmitted. Wood tissue has a t_T equal to zero since wood does not transmit photons. Hemispherical tissue reflectance and transmittance are thus the integral of the tissue scattering phase function over the appropriate azimuth (ϕ) and zenith ($\mu = \cos\theta$) angles:

$$r_T^{\pm}(\Omega',\Omega_T) = \int_{\phi'}\int_{\mu'} f(\Omega,\Omega';\Omega_T)\,d\mu' d\phi'$$
$$t_T^{\pm}(\Omega',\Omega_T) = \int_{\phi'}\int_{\mu'} f(\Omega,\Omega';\Omega_T)\,d\mu' d\phi' \quad (5)$$

where the (+) and (-) represent the adaxial and abaxial leaf surfaces, respectively. Finally, the single-scatter albedo of each tissue element (leaf, wood and litter surface) is denoted as:

$$\omega_T = r_T^{\pm} + t_T^{\pm} \quad (6)$$

Hemispherical reflectance and transmittance spectra are taken from databases representing arid and semi-arid vegetation (Asner et al. 1998), tropical and temperate grassland vegetation (Asner 1998, Asner et al. 1999), temperate forest vegetation (Lobell et al. in press), and tropical forest vegetation (Asner, *unpub. data*). Currently, these databases contain over 11,000 spectra and are being expanded through continuing field work. Sample spectra from the arid and semi-arid database of leaf and standing litter optical properties are shown in Figure 2.

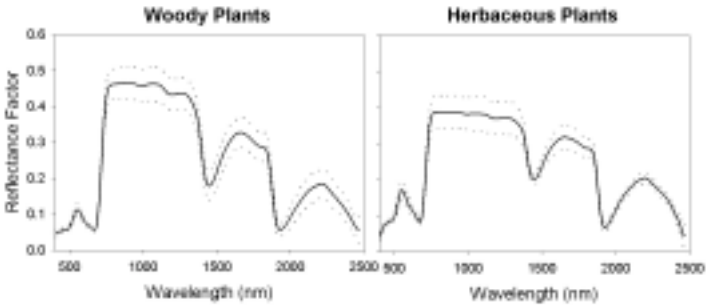

Figure 2. Leaf hemispherical reflectance spectra (mean and +/- 1 s.d.) of woody and herbaceous plants from 17 arid and semi-arid systems.

2.3 Single Photon Scattering by a Canopy

The model uses the formulation outlined by Verstraete et al. (1990) to exactly express photon single scattering in a canopy:

$$\rho_{\sin scat}(\Omega',\Omega) = \frac{\Gamma(\Omega',\Omega)}{|\mu'|\,\mu}\int_P \Im'(p)\Im(p)dp \tag{7}$$

where the gamma function (Γ) is the area scattering phase function, $\Im''$ is the direct solar radiation transmission, and $\Im$ is the transmission of scattered radiation. Unlike Verstraete et al. (1990), this process is integrated over the canopy plant area index (P), which is the sum of leaf (LAI), wood (WAI), and standing litter (LittAI) area indices (Asner 1998). An important part of this formulation for single photon scattering is that the so-called hotspot or retro-solar effect (when $\Omega' = \Omega$) is accounted for explicitly.

The gamma or area scattering phase function is well-known in canopy radiative transfer work (e.g., Myneni et al. 1989) and is given as:

$$\Gamma(\Omega',\Omega) = \frac{1}{2\pi}\int_{2\pi} f(\Omega',\Omega;\Omega_T)\, g_T(\Omega_T)\,|\cos\Omega_T\Omega'|\,d\Omega_T \tag{8}$$

where $f(\Omega',\Omega;\Omega_T)$ is the tissue scattering function (equation 4), and $g_T(\Omega_T)$ is the tissue orientation distribution with respect to the upward facing hemisphere. A random azimuthal orientation is assumed for plant tissues, thus the orientation distribution function for each tissue type can be stated in terms of normal zenith angle only (θ_T). deWit (1965) and Bunnik (1978) offered several theoretical leaf inclination distribution functions useful for plant canopy radiative transport modeling:

Planophile:	$g_T(\theta_T) = 2/\pi(1+\cos 2\theta_T)$;	tissues mostly horizontal
Erectophile:	$g_T(\theta_T) = 2/\pi(1-\cos 2\theta_T)$;	tissues mostly vertical
Plagiophile:	$g_T(\theta_T) = 2/\pi(1+\cos 4\theta_T)$;	tissues mostly inclined at 45^o
Uniform:	$g_T(\theta_T) = 2/\pi$;	random tissue orientation

(9)

More recently, Strebel et al. (1985) applied the continuous two-parameter beta distribution formula to describe the combined leaf inclination/azimuth angle distribution in a plant canopy.

The direct solar radiation tranmission $\Im''$ and scattered solar radiation transmission $\Im'$ are given by Verstraete et al. (1990):

$$\Im'(p) = e^{\left(-\frac{G(\Omega')}{|\mu'|}P\right)} \qquad \Im(p) = e^{\left(-\frac{G(\Omega)}{\mu}\frac{V_2(\Omega'\Omega,P)}{V(\Omega,P)}P\right)} \tag{10}$$

where

$$\frac{V_2(\Omega'\Omega,P)}{V(\Omega,P)} = \left(1-\frac{4}{3\pi}\right)\frac{P}{P_i} \qquad if\ P < P_i$$

$$= 1-\frac{4}{3\pi}\frac{P_i}{P} \qquad if\ P \geq P_i$$

Importantly, $P_i = 2r\Lambda/Geo(\Omega'\Omega)$, Λ is tissue area density (m^2/m^3), r is the radius of the sun-flecks on the illuminated tissue, and $Geo(\Omega'\Omega)$ is a function describing the geometry:

$$Geo(\Omega',\Omega) = \sqrt{\tan(\theta')^2 + \tan(\theta)^2 - 2\tan(\theta')\tan(\theta)\cos(\phi'-\phi)} \tag{11}$$

The *G*-function describes the total tissue area that is projected in a specific direction (Ω_X) by a unit canopy area, and this canopy area has a distribution function of tissue normal orientation which is identified by $g_T(z,\Omega_T)$, where *z* is the depth from the top of the canopy:

$$G(z,\Omega_X) = \frac{1}{2\pi}\int_0^{2\pi}\int_0^1 g_T(z,\Omega_T)|\cos\Omega_T\Omega_X\ |d\Omega_T \tag{12}$$

For some tissue orientations, the *G*-function can be solved analytically. For instance, random, vertical, and horizontal orientations produce *G* values of 0.5, $2/\pi\sqrt{1-\mu_T^2}$, and μ_T, respectively.

2.4 Photons Unscattered Until Reaching the Soil/Litter Surface

Photons that travel through the vegetation canopy without interception and which collide with the soil or litter surface are modeled according to Iaquinta and Pinty (1995), but modified to allow for multiple types of tissues such as foliage and wood:

$$\rho_{unscat}(\Omega'\Omega) = \rho_{surface}\Im'(P)\Im(P) = \rho_{surface}\, e^{\left[-\left(\frac{G(\Omega')}{|\mu u'|}+\frac{G(\Omega)V_2(\Omega'\Omega,P)}{\mu\quad V(\Omega,P)}\right)P\right]} \tag{13}$$

Surface soil and litter hemispherical reflectance is an input to the model, and is contained in databases constructed by Asner (1998), Asner et al. (1998,1999,2000), and Asner and Lobell (2000). Sample spectra from the arid and semi-arid region soil spectral database are shown in Figure 3.

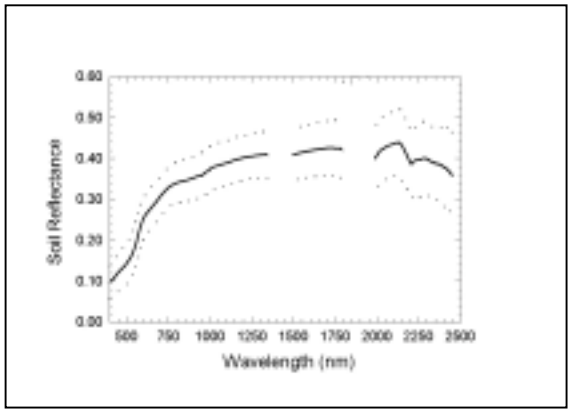

Figure 3. Sample soil reflectance spectra from 17 arid and semi-arid sites in North and South America. Solid line is the mean spectrum, and dotted lines are +/- 1 standard deviation from spectral database.

2.5 Photons Multiply Scattered in the Canopy

One of the most computationally expensive components of a physical model of radiation transport is the treatment of multiple scattering by plant tissues. Several models have been developed to solve the multiple scattering component of the radiative transfer equation (Shultis and Myneni 1988, Myneni and Asrar 1993, Knyazikhin et al. 1993). These models simulate photon scattering in many 'streams', often 48 or 96 in the unit sphere. This makes for a computationally demanding algorithm that can be difficult to employ when simulating many spectral bands or many pixels. Iaquinta and Pinty (1995) present a reasonable alternative that preserves much of the interaction depicted in the more mechanistic models in which multiple scattering is assumed to occur equally in angles exiting the canopy:

$$\rho_{multsc}(\Omega') = \frac{1}{|\mu'|}\int_{0\to 1} I^{M}(\mu')\mu' d\mu' \tag{14}$$

where I^M represents the source term within the canopy that consists of upward-traveling photons from the soil surface, singly scattered photons from all directions, and multiply scattered photons from all directions. A detailed description of I^M is given by Iaquinta and Pinty (1995; Appendix 1).

2.6 Inter-canopy Shadowing

Sections 2.1-2.5 describe radiation transport in one dimension – a theoretical slab of infinitesimally small scatters represents multiple plant tissue types. Several 3-dimensional radiative transfer models have been developed (e.g., Myneni and Asrar 1993), allowing for the representation of multiple canopies and in-homogeneous canopy coverage. These 3-D models are computationally expensive, which severely limits their inversion using numerical optimization techniques.

Li and Strahler (198x) developed a crown shadowing model that simulates the silhouette shadow cast by an overstory canopy onto the ground or understory. This model is computationally efficient. For a given illumination and viewing geometry, crown dimensions, and stand density (number of crowns per pixel), the fraction of sunlit crown, sunlit understory, and shaded understory seen by the observer is calculated (Figure 4). This provides a convenient means to estimate the fraction of sunlit and shaded canopy and understory that is apparent to the observer.

Figure 4. Geometric-optical shadow model estimates sunlit and shaded crown and understory based on crown macro-properties and Sun-viewing geometry.

2.7 Crown Silhouette Transmission

Radiation reaching the understory or ground level within the crown shadow silhouette described in Section 2.6 can arrive from singly scattered sources, multiply scattered sources, or directly (as uncollided radiation). Thus, equation (13) can be used to estimate the reflectance of the viewable ground shadow fraction of the simulated pixel.

2.8 Pixel-scale Reflectance

For any number of vegetation/crown types, the 1-D radiation transport is simulated based on Sections 2.1-2.5. Distributions representing the pixel density and crown dimensions of these 1-D 'slabs' are then input into the inter-canopy shadow model (Section 2.6), and crown silhouette transmission is estimated (Section 2.7). The pixel-level reflectance is then summed:

$$\rho_{pixel}(\Omega'\Omega) = \left(\sum_{v} \rho^{v}_{sunlitcanopy}(\Omega'\Omega) \cdot F^{v}_{sunlitcanopy} \right) + \rho_{shadedcanopy}(\Omega'\Omega) \cdot F_{shadedcanopy} \quad (15)$$

Note that although equation 15 is linear, it contains fully non-linear mixing in component ρ via radiation transport model and in component F via crown geometric-optical model.

2.9 Atmospheric Radiative Transfer

An atmospheric radiative transfer code is needed to scale the top-of-canopy or landscape surface reflectance (Section 2.8) to top-of-atmosphere radiance. A number of codes are available, and the 6S model of Vermote et al. (1996) provides realistic simulation of water vapor, aerosol, and molecular gas interactions. Examples of atmospheric absorption spectra from 6S are provided in Figure 5.

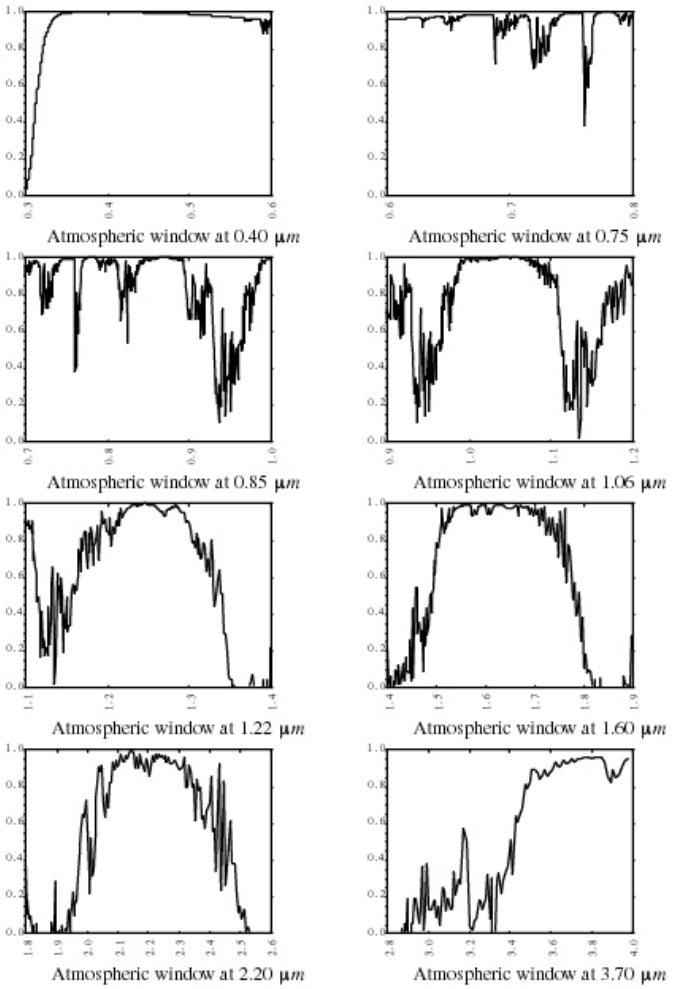

Figure 5. Sample water vapor absorption spectra derived from 6S code (Vermote et al. 1996).

2.10 Spatial Database and Model Setup

The model can be run for a single pixel or to create a simulated image. For the latter, a method is required to provide spatial context for soil and vegetation parameters. Soil maps can be linked to soil spectra; Vegetation maps can be used to constrain model inputs of tissue area indices, tissue angle distributions, stand density, crown dimensions, etc. A Normalized Difference Vegetation Index (NDVI) image from an actual scene can also be used to spatially scale the LAI inputs to the model from pixel to pixel. An overall list of model inputs and potential sources is shown in Table 1.

Table 1. Model input parameters and data sources.

Model Parameter	Source
Tissue optical properties	Spectra databases
Tissue area indices	Keyed to vegetation map and NDVI
Tissue angle distributions	By vegetation type, keyed to vegetation map
Vegetation/stand density	Keyed to vegetation map
Vegetation crown dimensions	Keyed to vegetation map
Sun geometry	Selected as input
Viewing geometry	Based on AVIRIS, Hyperion, etc FOV characteristics and flight orientation
Soil reflectance	By soil type, keyed to soil map
Atmospheric Properties	Selected as input

3. Sample Model Output

Component output of the model has been presented by Asner (1998) and Asner et al. (1999). The effect of changing stand density on understory photon interception in a simulated savanna is shown in Figure 6a. The effect of increasing LAI, while all of other parameters are held constant and without an atmosphere, is shown in Figure 6b.

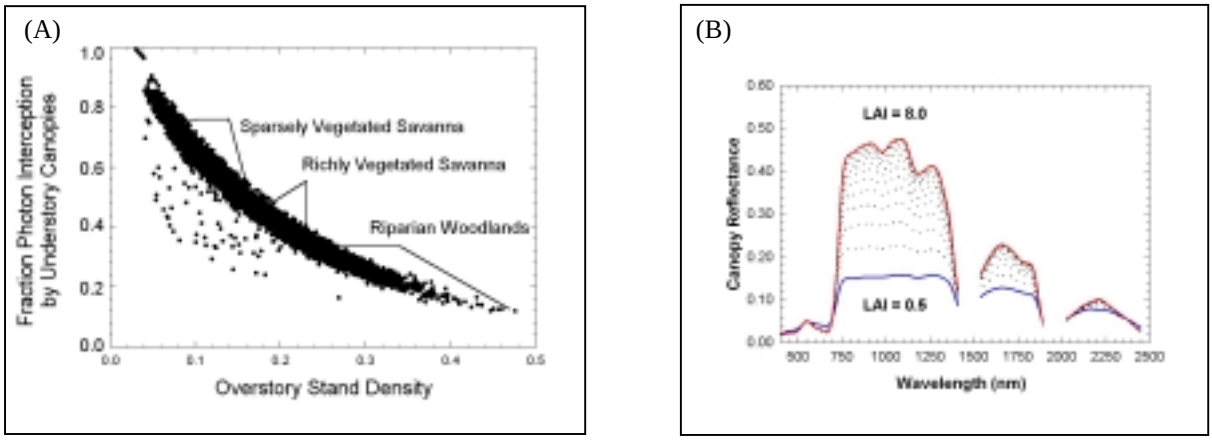

Figure 6. (A) Simulated effect of overstory stand density on understory photon interception. (B) Simulated effect of LAI on canopy reflectance.

The model has undergone testing in shrubland, grassland, tropical forest, and temperate forests scenarios. Sample output is shown in Figure 7 for a temperate coniferous site in central Oregon. Actual AVIRIS flightline and solar geometry from June 10, 1999 were used. Needle and wood optical properties were collected in the field using a full-range spectroradiometer (Analytical Spectra Devices, Inc.) and an integrating sphere designed for vegetative tissue analysis. Stand density, crown dimensions, LAI, PAI, and tissue angle distributions were also collected. The simulated data were scaled to a NDVI image from AVIRIS. Atmospheric parameters were taken from typical mid-latitude continental conditions, and aerosol optical thickness at 550 nm was given as 0.05.

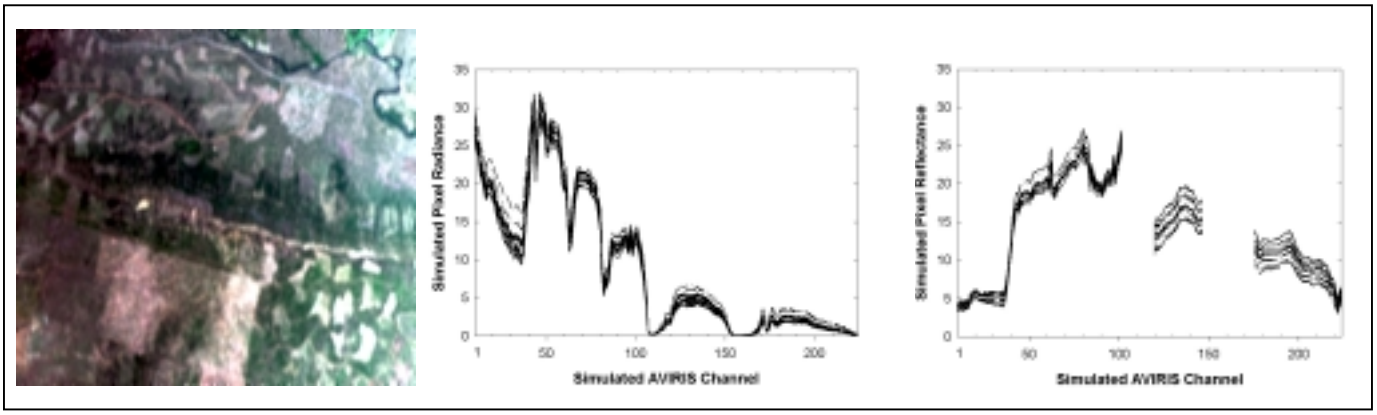

Figure 7. (Left) Simulated false color AVIRIS image; (Center) Sample simulate top-of-atmosphere radiance in AVIRIS channels; (Right) Simulated apparent surface reflectance in AVIRIS channels.

4. Inverse Modeling

Both the 1-D (Sections 2.1-2.5) and quasi 3-D (Sections 2.1-2.10) models can be inverted to estimate parameters of interest. The inversion is accomplished numerically by iteratively adjusting model parameters until the minimum difference between actual (e.g., AVIRIS) and modeled spectra is achieved (Figure 7; center). In particular, the 1-D model can be inverted by constraining tissue optical properties to known ranges from the spectral databases. The leaf, litter and wood area indices (LAI, LitterAI, WoodAI) can then be estimated. Examples are shown for a shrubland ecosystem in Texas (Figure 8a) and a tropical grassland in Brazil (Figure 8b).

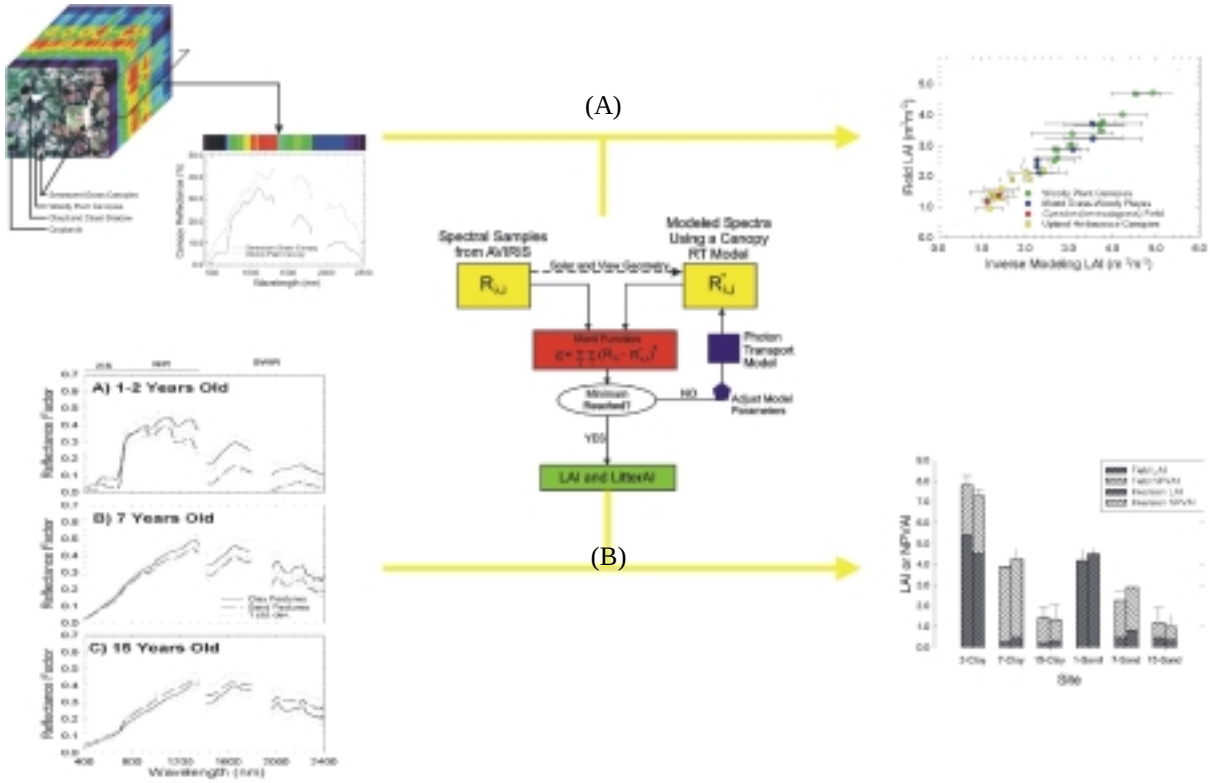

Figure 8. (A) Inverse modeling was used to estimate leaf area index (LAI) in a Texas shrubland (from Asner et al. 1998). (B) A similar approach was used to estimate grassland LAI and LitterAI in Brazil (from Asner et al. 1999).

5. Conclusions

A model has been developed to simulate hyperspectral reflectance and radiance data of terrestrial ecosystems. The critical components of the model include large spectral databases of vegetative tissues (foliage, wood, litter) and soils, a fast hybrid canopy radiative transfer/geometric-optical model, and an atmospheric radiative transfer code. The tissue and soil spectral databases cover the pertinent part of the shortwave spectrum (400-2500nm) and are continually being expanded via ongoing field work. The photon transport model is based on work by Verstraete et al. (1990), Iaquinta and Pinty (1995), Asner (1998), and Li and Strahler (1985). It is fast and is thus adequate for hyperspectral simulations over thousands of image pixels. It can also be inverted to retrieve certain land-surface variables such as tissue area indices. Planned improvements include a physical soil spectral model that includes a mechanistic representation of soil moisture and organic matter.

6. Acknowledgements

This work was supported by NASA New Investigator Program grant NAG5-8709.

7. References

Asner, G.P. (1998), Biophysical and biochemical sources of variability in canopy reflectance, *Remote Sens. Environ.* 64:234-253.

Asner, G.P., Townsend, A.R., and Bustamante, M.C.C. (1999), Spectrometry of pasture condition and biogeochemistry in the Central Amazon. *Geophys. Res. Lett.* 26: 2769-2772.

Asner, G.P., Wessman, C.A., Bateson, C.A., and Privette, J.L. (2000), Impact of tissue, canopy and landscape factors on reflectance variability of arid ecosystems. *Rem. Sens. Environ.*

Asner, G.P., Wessman, C.A., and Schimel, D.S. (1998), Heterogeneity of savanna canopy structure and function from imaging spectrometry and inverse modeling, *Ecol. Applic.* 8:1022-1036.

Breece, H.T. and Holmes, R.A. (1971), Bidirectional scattering characteristics of healthy green soybean and corn leaves in vivo. *Appl. Optics* 10: 119-127.

deWit, C.T. (1965), Photosynthesis of leaf canopies. Pudoc Publ, Wageningen, The Netherlands.

Goel, N.S. (1988), Models of vegetation canopy reflectance and their use in estimating biophysical parameters from reflectance data. *Rem. Sens. Rev.* 4: 1-212.

Iaquinta, J., and Pinty, B. (1994), Adaptation of a bidirectional reflectance model including the hotspot to an optically thin canopy. *Proc. Sixth ISPRS Int'l Symp. Phys. Meas. Sig. Rem. Sens*. 683-690.

Jacquemoud, S. (1993), Inversion of the PROSPECT+SAIL canopy reflectance model from AVIRIS equivalent spectra: theoretical study. *Rem. Sens. Environ.* 44: 281-292.

Li, X. and Strahler, A. (1985), Geometrical-optical modeling of a coniferous forest canopy. *IEEE Trans. Geosci. Rem. Sens*. 23: 207-221.

Lobell, D.B., Asner, G.P., Law, B.E. and Treuhaft, R.N. Sub-pixel cover estimation of coniferous forests in Oregon using SWIR imaging spectrometry. *J. Geophys. Res.*, in press.

Myneni, R.B., Nemani, R.R., and Running, S.W. (1997), Estimation of global leaf area index and absorbed PAR using radiative transfer models, *IEEE Trans. Geosci. Rem. Sens*. 35:1380-1396.

Myneni, R.B. and Asrar, G. (1993), Radiative transfer in three-dimensional atmosphere-vegetation media. *J. Quant. Spectrosc. Radiat. Transfer*, 49: 585-598.

Myneni, R.B., Ross, J., and Asrar, G. (1989), A review of the theory of photon transport in leaf canopies. *Agric. For. Meteorol.*, 45: 1-153..

Privette, J.L., Emery, W.J., and Schimel, D.S. (1996), Inversion of a vegetation reflectance model with NOAA AVHRR data. *Rem. Sens. Environ.* 58: 187-200.

Shultis, J.K. and Myneni, R.B. (1988), Radiative transfer in vegetation canopies with anisotropic scattering. *J. Quant. Spectrosc. Radiat. Transfer* 39: 115-129.

Strebel, D.E., Goel, N.S., and Ranson, K.J. (1985), Two-dimensional leaf orientation distributions. *IEEE Trans. Geosci. Rem. Sens*. 23: 640-646.

Vermote, E.F., et al. (1996), Second simulation of the satellite signal in the solar spectrum, 6S: an overview. *IEEE Trans. Geosci. Rem. Sens*. 35: 675-699.

Verstrate, M.B., Pinty, B., and Dickinson, R.E. (1990), A physical model of the bidirectional reflectance of vegetation canopies, 1. Theory. *J. Geophys. Res.* 95: 755-765.